

# Non-Arrhenius conductivity in the fast lithium conductor $\text{Li}_{1.2}\text{Ti}_{1.8}\text{Al}_{0.2}(\text{PO}_4)_3$ : A $^7\text{Li}$ NMR and electric impedance study

K. Arbi,<sup>1</sup> M. Tabellout,<sup>2</sup> M. G. Lazarraga,<sup>1</sup> J. M. Rojo,<sup>1</sup> and J. Sanz<sup>1,\*</sup>

<sup>1</sup>*Instituto de Ciencia de Materiales de Madrid (ICMM), Consejo Superior de Investigaciones Científicas (CSIC), Cantoblanco, 28049 Madrid, Spain*

<sup>2</sup>*Laboratoire de Physique de l'Etat Condensé (LPEC), UMR CNRS 6087 Université du Maine, Av. O. Messiaen 72085 Le Mans Cedex 9, France*

(Received 17 November 2004; revised manuscript received 30 March 2005; published 9 September 2005)

Lithium ion motion has been investigated in the  $\text{Li}_{1.2}\text{Ti}_{1.8}\text{Al}_{0.2}(\text{PO}_4)_3$  compound with NMR and impedance spectroscopies. From the analysis of the bulk dc conductivity ( $\sigma_{b,dc}$ ) and the frequency at the maximum ( $\omega_{pp}$ ) of the imaginary electric modulus, two regimes for lithium motion have been identified. From the analysis of the temperature dependence of  $^7\text{Li}$  NMR quadrupole constant ( $C_Q$ ) and spin-spin relaxation rate ( $T_2^{-1}$ ), the evolution of  $M_1$  and  $M_2$  sites occupancy in the conduction network of the fast ion conductor has been deduced. At low temperatures ( $T < 250$  K), differences in activation energies deduced from NMR ( $E_m^R = 0.19$  eV) and conductivity ( $E_M^C = 0.31$  eV) are discussed in terms of a correlated lithium motion. In this regime, the  $\beta$  parameter that relates both energies ( $E_m = \beta E_M$ ) takes the value 0.61. In the high temperature regime ( $T > 250$  K), the activation energy  $E_M$  deduced by the two techniques show similar values (0.22 eV). In this case the  $\beta$  parameter is nearly equal to 0.85. From the NMR results, it has been concluded that the partial cancellation of the correlation in lithium motion is associated with the creation of vacancies at  $M_1$  sites. On the other hand, some differences in  $\beta$  and  $\tau_0$  parameters have been detected, indicating that relaxation functions are slightly different in two techniques. In particular, the NMR  $\beta^R$  correlation factor is slightly higher and the NMR  $\tau_0^R$  parameter is almost one order of magnitude higher than that deduced from electric measurements.

DOI: [10.1103/PhysRevB.72.094302](https://doi.org/10.1103/PhysRevB.72.094302)

PACS number(s): 66.30.Hs, 66.10.Ed, 76.60.Es

## I. INTRODUCTION

Much effort has been devoted during the last few decades to understand the ion dynamics in Li conducting materials. In this context, NMR spin lattice relaxation (SLR) and electrical conductivity (EC) measurements are useful tools to analyze Li motions. In fast ion conductors, it is usually found that relaxation functions describing SLR and EC data deviate from the ideal BPP (Bloembergen, Purcell, and Pound) and Debye behaviors. From the analysis of NMR and EC relaxations, correlation effects affecting Li motion can be estimated. In particular, the coupling model predicts a crossover time  $t_c$  below which ions behave as independent single particles but above it, the ions motion is correlated.<sup>1</sup> Activation energies in the two regimes  $E_m$  and  $E_M$  satisfy the relation  $E_m = \beta E_M$ , where  $\beta$  is the factor that takes into account the correlations effects in ions motion ( $0 < \beta < 1$ ). In the absence of correlation,  $\beta$  parameter takes the value 1, and  $E_m = E_M$ .

On the other hand, it has been shown that some glasses which are fast ion conductors show a temperature dependence of conductivity that display important deviations from the Arrhenius behavior. Ngai and Rizo<sup>2</sup> proposed elimination of correlation effects at increasing temperatures as the reason for the non-Arrhenius behavior observed in glasses. In this sense, Robertson and West<sup>3</sup> have suggested that the influence of the structure on the mobile ions diminishes as the temperature increases and that the conductivity of the best Li ion conductors goes toward a common value close to  $10^{-1}$  S cm<sup>-1</sup>. Among the crystalline fast ion conductors, the Nasicon-type compounds  $\text{Li}_{1+x}\text{Ti}_{2-x}\text{Al}_x^{3+}(\text{PO}_4)_3$  (Refs. 4–6) display one of the highest Li-conductivities measured at

room temperature, the activation energy  $E_M^C$  decreasing toward a minimum value of 0.30 eV for  $x \geq 0.2$ .

The Nasicon-type structure is formed by  $\text{M}_2(\text{PO}_4)_3$  units in which  $\text{MO}_6$  octahedra share corners with  $\text{PO}_4$  tetrahedra. The ideal framework displays the rhombohedral symmetry (space group  $R\bar{3}c$ ) but in some particular cases a triclinic distortion (space group  $C\bar{1}$ ) has been detected.<sup>7–9</sup> In the network of the rhombohedral phases, alkaline ions can occupy two different sites: (1)  $M_1$  sites located at trigonal  $c$  axes, with a sixfold oxygen coordination and (2)  $M_2$  sites symmetrically distributed around the trigonal axes, with a 10-fold oxygen coordination (Fig. 1). Taking into account the Li ion size, the  $M_2$  site is not suitable and the Li ions are situated in a fourfold coordination at intermediate  $M_{1/2}$  positions between  $M_1$  and  $M_2$  sites.<sup>7–10</sup> The ionic conductivity of the rhombohedral phase is higher and the activation energy lower than that of the triclinic phase.

In this paper we have undertaken a comparative analysis of the NMR and conductivity data in the rhombohedral  $\text{Li}_{1.2}\text{Ti}_{1.8}\text{Al}_{0.2}(\text{PO}_4)_3$ , the data being recorded in a large interval of frequency and temperature. In that compound, the temperature dependence of the conductivity displays the non-Arrhenius behavior reported in other fast ion conductors. NMR spectroscopy has been used to estimate the occupancy of the structural sites by Li ions as temperatures increase. The comparison of results obtained by NMR ( $1/T_1$  and  $1/T_2$  relaxation rates) and electric measurements (relaxation time and dc conductivity) has permitted us to get a better understanding of the Li motion in Nasicon-type compounds.

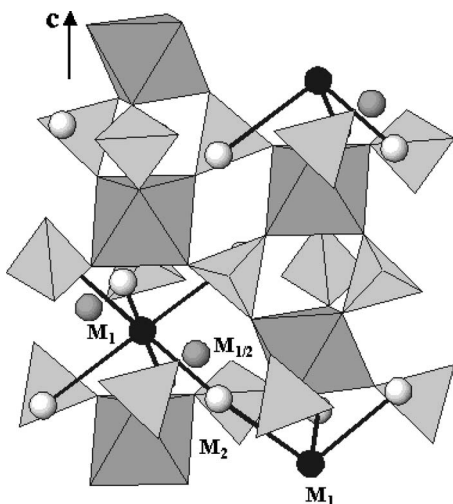


FIG. 1. Rhombohedral structure of Nasicon compounds showing structural  $M_1$ ,  $M_{1/2}$ , and  $M_2$  sites susceptible to be occupied by lithium.

## II. EXPERIMENTAL SECTION

The ionic conductor  $\text{Li}_{1.2}\text{Ti}_{1.8}\text{Al}_{0.2}(\text{PO}_4)_3$  was prepared following the method described elsewhere.<sup>6,11</sup> X-ray diffraction was used to assess purity of prepared samples. X-ray powder diffraction patterns were recorded with the  $\text{Cu } K\alpha$  radiation ( $\lambda = 1.5405981 \text{ \AA}$ ) at different temperatures in the range of 25–500 °C, using a high-temperature AP HTK10 camera adapted to a PW 1050/25 Phillips diffractometer. In cooling and heating runs, the sample was kept at each temperature for 10 min before x-ray diffraction (XRD) patterns were recorded. Data were collected in the  $2\theta$  range 10–70° with a step size of 0.02° and a counting time of 0.1 s/step.

Impedance measurements were made on cylindrical pellets of 13 mm diameter and approximately 1.4 mm thickness. Pellets were first compacted by cold pressing at 3 MPa, then they were sintered at 950–1000 °C for 24 h. For the electric measurements platinum electrodes were deposited by sputtering on the two faces of the pellet. Impedance measurements were performed over the frequency range  $10^{-1}$ – $1.8 \times 10^9$  Hz at increasing temperatures (150–500 K). To cover the full frequency domain, two experimental setups were used: from  $10^{-1}$  to  $10^6$  Hz a Solartron SI 1260 combined with a broadband dielectric converter (BDC) was used; for the high frequency range ( $10^6$ – $1.8 \times 10^9$  Hz) an HP 4291A rf impedance analyzer was used with a precision coaxial line for which propagation parameters are well known. In this case, the sample was located at the end of the line and the temperature dependence of the electric impedance was then deduced from the analysis of the complex reflection factor as a function of temperature. In both cases, the sample temperature was measured with accuracies better than  $\pm 0.1$  K.

$^7\text{Li}$  (Magical Angle Spinning) NMR spectra were recorded at room temperature in a MSL-400 Bruker spectrometer (9.4 T). The frequency used for  $^7\text{Li}$  was 155.50 MHz. The sample was spun at 4 kHz during signal recording. The spectra were obtained after  $\pi/2$  pulse irradiation ( $\approx 4 \mu\text{s}$ ) with a recycling time of 10 s. The number of scans was in

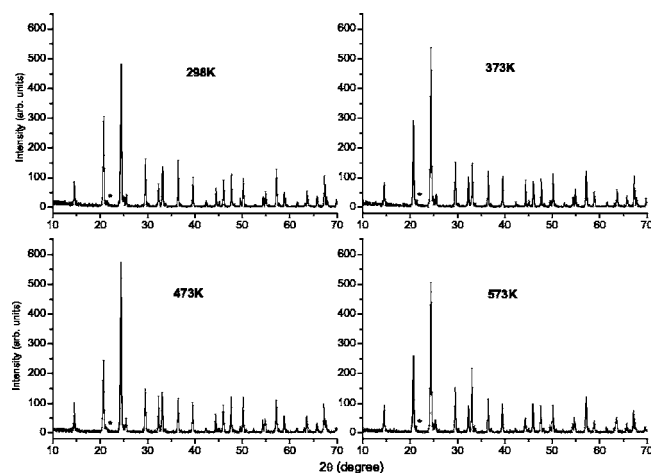


FIG. 2. X-ray diffraction patterns of  $\text{Li}_{1.2}\text{Ti}_{1.8}\text{Al}_{0.2}(\text{PO}_4)_3$  recorded at increasing temperatures. The small peak detected at  $2\theta \sim 22^\circ$  (labeled with an asterisk) corresponds to the secondary  $\text{AlPO}_4$  phase.

the range of 100–800. In the temperature range 100–450 K, quadrupole interactions deduced from  $^7\text{Li}$  spectra remain small ( $C_Q < 70$  kHz), making the irradiation of the central and satellite transitions nonselective.  $^7\text{Li}$  chemical shift values were given relative to 1M LiCl aqueous solution. The fitting of the NMR spectra was made with the Bruker WINFIT software package.<sup>12</sup>  $^7\text{Li}$  spin-lattice relaxation times ( $T_1$ ) were measured with the  $\pi - \tau - \pi/2$  sequence at 11 MHz in a SXP 4/100 spectrometer. In all temperatures analyzed, the recovery of magnetization was exponential. Reciprocal spin-spin relaxation times ( $T_2^{-1}$ ) values were calculated from the full-width at half-maximum (FWHM) of the central NMR lines recorded in static conditions. In the case of Gaussian lines,  $T_2^{-1}$  was calculated as  $0.6\pi$  times the FWHM; in the case of Lorentzian lines,  $T_2^{-1}$  was calculated as  $\pi$  times the FWHM.

## III. RESULTS

### A. X-ray diffraction study

XRD patterns of  $\text{Li}_{1.2}\text{Ti}_{1.8}\text{Al}_{0.2}(\text{PO}_4)_3$  recorded at increasing temperatures are given in Fig. 2. The most intense reflections correspond to the rhombohedral ( $R\bar{3}c$ ) Nasicon phase; however, the small reflection detected at  $2\theta \approx 22^\circ$  (labeled with an asterisk) has been ascribed to the formation of the secondary phase  $\text{AlPO}_4$ . The heating of the sample only produced the peaks shift associated with the expansion of the lattice. In this analysis, no phase transition involving the previously reported triclinic distortion<sup>7–9</sup> was detected.

### B. Conductivity

The angular frequency ( $\omega$ ) dependence of the conductivity ( $\sigma'$ ) at different temperatures is shown in Fig. 3. At 273 K the plateau detected in the frequency range  $10^0$ – $10^3 \text{ s}^{-1}$ , followed by a dispersive regime at around  $10^6 \text{ s}^{-1}$ , is ascribed to the grain boundary response. Another plateau is observed in the frequency range  $10^7$ – $10^9 \text{ s}^{-1}$  that corre-

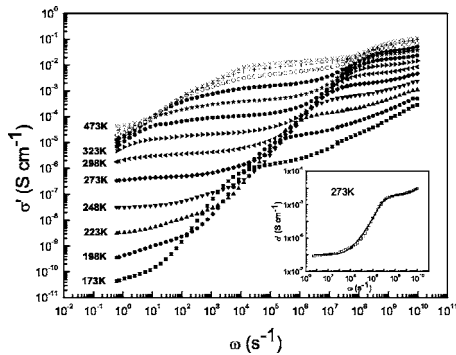


FIG. 3. Real conductivity vs angular frequency at indicated temperatures for the  $\text{Li}_{1.2}\text{Ti}_{1.8}\text{Al}_{0.2}(\text{PO}_4)_3$  sample. The inset corresponds to the best fitting of data taken at 273 K.

sponds to grain interior (bulk) response. At higher temperatures ( $T > 300$  K) an ill-defined dispersive regime is observed below  $10^2 \text{ s}^{-1}$  that is ascribed to the blocking of the ions ( $\text{Li}^+$  in this work) at the electrodes of the pellet.<sup>13</sup>

The experimental  $\sigma'(\omega)$  data were fitted taking into account the grain interior and the grain boundary responses. For the grain interior (bulk) we assumed that the complex conductivity takes the form

$$\hat{\sigma}_b = \sigma_{b,\text{dc}} \left[ 1 + \left( \frac{i\omega}{\omega_{bp}} \right)^n \right] + i\omega\varepsilon_\infty, \quad (1)$$

where  $\sigma_{b,\text{dc}}$  accounts for the conductivity measured at the plateau,  $\omega_{bp}$  is the transition frequency from the plateau to the dispersive regime,  $n$  is the correlation parameter, and  $\varepsilon_\infty$  is the permittivity at  $\omega \rightarrow \infty$ . For the grain boundary, we assumed that the complex conductivity takes the form  $\hat{\sigma}_g = \sigma_{g,\text{dc}} [1 + (i\omega/\omega_{gp})]$ , where the parameters  $\sigma_{g,\text{dc}}$  and  $\omega_{gp}$  have similar meanings to those of the former equation. The fitting equation used was  $\hat{\sigma} = (1/\hat{\sigma}_b + 1/\hat{\sigma}_g)^{-1}$ , where  $\hat{\sigma}$  ac-

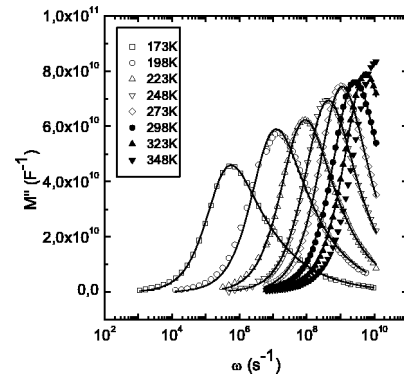


FIG. 4. Imaginary part of the electric modulus vs angular frequency at indicated temperatures for  $\text{Li}_{1.2}\text{Ti}_{1.8}\text{Al}_{0.2}(\text{PO}_4)_3$ . The best fittings to modulus peaks are also given (solid lines).

counts for the overall conductivity. As an example, the fitting obtained at 273 K is shown in the inset of Fig. 3 (solid line). This analysis allowed us to determine the grain interior dc conductivity whose values are outlined in Table I.

Figure 4 shows the imaginary part of the electric modulus ( $M''$ ) as a function of the angular frequency ( $\omega$ ) at several temperatures. We can see that the  $M''$  peak shows an asymmetry toward high frequency, which has been ascribed to correlation effects in the motion of the mobile ions.<sup>14,15</sup> The entire  $M''$  peaks were fitted to the equation  $\hat{M} = i\omega/\hat{\sigma}_b$ , where  $\hat{\sigma}_b$  has been already defined in Eq. (1). For the fitting we have not taken into account the grain boundary response because its contribution to  $M''(\omega)$  is negligible. The fittings obtained are shown in Fig. 4 (solid lines) and the fitting parameters  $\omega_{bp}$  and  $n$  are outlined in Table I.

Figure 5 shows the plot of  $\sigma_{b,\text{dc}} T$  vs  $1000/T$ , where  $\sigma_{b,\text{dc}}$  is the grain interior (bulk) dc conductivity and  $T$  is the absolute temperature. The experimental data depart from a unique linear dependence and were fitted to two equations of the form<sup>16</sup>

TABLE I. Conductivity  $\sigma_{b,\text{dc}}$  ( $\text{S cm}^{-1}$ ), frequency  $\omega_{bp}$  ( $\text{s}^{-1}$ ), and correlation  $\beta^C$  (dimensionless) parameters deduced from fittings of  $\sigma'(\omega)$  and  $M''(\omega)$  values taken at different temperatures.  $C_Q$  (kHz) and  $P_1$  and  $P_2$  (dimensionless) values deduced from  $^7\text{Li}$  NMR spectra recorded at increasing temperatures.

$T$ (K)	EC			$\beta^C = 1 - n$	NMR		
	$\sigma_{b,\text{dc}}$ ( $\text{S cm}^{-1}$ )	$\omega_{bp}$ ( $\text{s}^{-1}$ )	$n$		$C_Q$ (kHz)	$P_1$	$P_2$
173	$1.5 \pm 0.2 \times 10^{-6}$	$4.24 \pm 0.03 \times 10^5$	$0.60 \pm 0.01$	$0.40 \pm 0.01$			
198	$2.0 \pm 0.3 \times 10^{-5}$	$8.5 \pm 0.1 \times 10^6$	$0.57 \pm 0.01$	$0.43 \pm 0.01$	$35.7 \pm 0.4$	$0.96 \pm 0.01$	$0.07 \pm 0.01$
223	$1.4 \pm 0.2 \times 10^{-4}$	$5.36 \pm 0.04 \times 10^7$	$0.51 \pm 0.01$	$0.49 \pm 0.01$	$37.7 \pm 0.5$	$0.94 \pm 0.01$	$0.08 \pm 0.01$
248	$6 \pm 1 \times 10^{-4}$	$2.46 \pm 0.03 \times 10^8$	$0.47 \pm 0.01$	$0.53 \pm 0.01$	$37.9 \pm 0.5$	$0.93 \pm 0.01$	$0.08 \pm 0.01$
273	$2.0 \pm 0.3 \times 10^{-3}$	$5.98 \pm 0.06 \times 10^8$	$0.43 \pm 0.01$	$0.57 \pm 0.01$	$40.5 \pm 0.6$	$0.90 \pm 0.01$	$0.09 \pm 0.01$
298	$4.8 \pm 0.5 \times 10^{-3}$	$1.40 \pm 0.02 \times 10^9$	$0.40 \pm 0.01$	$0.60 \pm 0.01$	$42.5 \pm 0.6$	$0.88 \pm 0.01$	$0.10 \pm 0.01$
323	$1.0 \pm 0.1 \times 10^{-2}$	$2.75 \pm 0.04 \times 10^9$	$0.34 \pm 0.01$	$0.66 \pm 0.01$	$45.7 \pm 0.6$	$0.84 \pm 0.01$	$0.11 \pm 0.01$
348	$1.9 \pm 0.2 \times 10^{-2}$				$48.3 \pm 0.6$	$0.81 \pm 0.01$	$0.12 \pm 0.01$
373	$2.8 \pm 0.5 \times 10^{-2}$				$51.3 \pm 0.7$	$0.78 \pm 0.01$	$0.13 \pm 0.01$
398	$3 \pm 1 \times 10^{-2}$				$53.3 \pm 0.7$	$0.76 \pm 0.01$	$0.14 \pm 0.01$
423	$5 \pm 1 \times 10^{-2}$				$55.7 \pm 0.8$	$0.73 \pm 0.01$	$0.15 \pm 0.01$
448	$7 \pm 2 \times 10^{-2}$				$59 \pm 0.8$	$0.69 \pm 0.01$	$0.16 \pm 0.01$

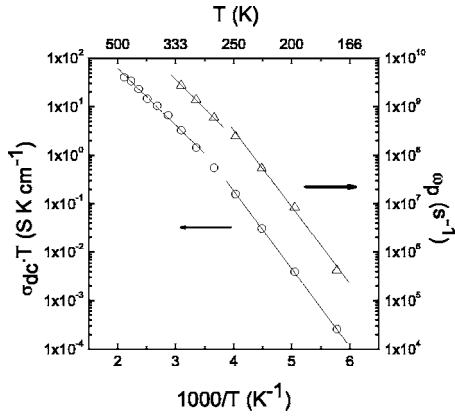


FIG. 5. Grain interior dc conductivity vs reciprocal temperature for  $\text{Li}_{1.2}\text{Ti}_{1.8}\text{Al}_{0.2}(\text{PO}_4)_3$ . The temperature dependence of the frequency ( $\omega_{bp}$ ) at the maximum of the modulus peak is also included.

$$\sigma_{b,\text{dc}}T = \sigma_{b,0} \exp(-E_M^C/kT), \quad (2)$$

where  $\sigma_{b,0}$  is a preexponential factor,  $E_M^C$  is the activation energy,  $k$  is the Boltzmann constant, and  $T$  is the absolute temperature. The fitting parameters (preexponential factor  $\sigma_{b,0}$  and activation energy  $E_M^C$ ) deduced for the two regimes, here called high temperature (250–400 K) and low temperature (170–250 K) regimes, are outlined in Table II. In Fig. 5 we have also plotted  $\omega_{bp}$  vs  $1000/T$ , where  $\omega_{bp}$  is the angular frequency at the maximum of the  $M''$  peak. In this plot, we also see two regimes in which experimental  $\omega_{bp}$  data were fitted to two equations of the form  $\omega_{bp} = \omega_{bp0} \cdot \exp(-E_\omega^C/kT)$ . The fitting parameters ( $\omega_{bp0}$  and  $E_\omega^C$ ) deduced for the two regimes are outlined in Table II. It can be seen that the activation energies  $E_M^C$  and  $E_\omega^C$  are almost coincident for each regime.

### C. $^7\text{Li}$ NMR signal

$^7\text{Li}$  NMR ( $I=3/2$ ) spectra of the  $\text{Li}_{1.2}\text{Ti}_{1.8}\text{Al}_{0.2}(\text{PO}_4)_3$  sample are formed by a central line ( $1/2, 1/2$  transition) and two satellite lines ( $-3/2, -1/2$  and  $1/2, 3/2$  transitions). In  $^7\text{Li}$  MAS-NMR spectra, satellite transitions were modulated by the sample rotation, detecting equally spaced bands separated by the spinning rate (see inset in Fig. 6). Spectra were fitted with the Bruker WINFIT program, which takes into account first-order quadrupole interactions. From this analysis, the quadrupole constant  $C_Q$  and the asymmetry parameter  $\eta$  were determined. The variation of the quadrupole constant

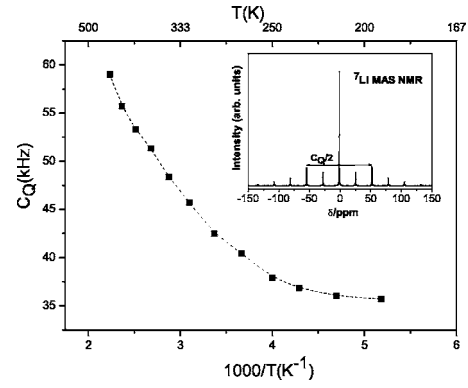


FIG. 6. Temperature dependence of the quadrupole  $C_Q$  constant deduced from  $^7\text{Li}$  NMR spectra of  $\text{Li}_{1.2}\text{Ti}_{1.8}\text{Al}_{0.2}(\text{PO}_4)_3$ . The  $^7\text{Li}$  MAS-NMR spectrum recorded at room temperature is given in the inset.

$C_Q$  as a function of the reciprocal temperature ( $1000/T$ ) is shown in Fig. 6.  $C_Q$  is nearly constant ( $\sim 36$  kHz) below 250 K, but above this temperature an increment of  $C_Q$  is observed. Below 175 K an important broadening of the satellite transitions makes difficult the determination of  $C_Q$  values. In all analyzed temperatures,  $\eta$  values are zero, indicating that sites occupied by Li ions display axial symmetry.

$T_2^{-1}$  (spin-spin) and  $T_1^{-1}$  (spin-lattice) relaxation rates, deduced from the central transition, are plotted vs reciprocal temperature in Fig. 7. In the 100–160 K range, the line shape of the central transition is Gaussian and  $T_2^{-1}$  remains constant. Below 120 K, the nearly constant  $T_1^{-1}$  was ascribed to the relaxation induced by paramagnetic impurities. Above 160 K, the line shape becomes Lorentzian as a consequence of the Li motion. When the temperature increases ( $160 < T < 210$  K),  $T_1^{-1}$  increases and  $T_2^{-1}$  decreases, the latter reaching a minimum at 210 K. At 260 K, a maximum of  $T_1^{-1}$  and  $T_2^{-1}$  is detected. At higher temperature,  $T_1^{-1}$  and  $T_2^{-1}$  decrease again indicating the onset of faster motions that reduces residence times at structural sites.

At the  $T_1^{-1}$  maximum, the residence time of Li ions at the occupied sites is  $\tau \approx \omega_0^{-1} \approx 1.4 \times 10^{-8}$  s ( $\omega_0 \tau = 1$ ). On the other hand, the temperature dependence of  $T_1^{-1}$  and  $T_2^{-1}$ , expressed in rad/s, can be described with the equations<sup>17,18</sup>

$$T_1^{-1} = C \left[ \frac{\tau}{1 + (\omega_0 \tau)^{1+\beta}} + \frac{4\tau}{1 + (2\omega_0 \tau)^{1+\beta}} \right], \quad (3)$$

TABLE II. Grain interior activation energies  $E_M^C$  and  $E_\omega^C$  (eV), preexponential factors  $\sigma_{b,0}$  ( $\text{S cm}^{-1}$ ),  $\omega_{bp0}$  ( $\text{s}^{-1}$ ), and  $\tau_0^C$  (s) deduced from conductivity and modulus data. High temperature correlation time  $\tau_0^R$  (s), correlation factors  $\beta^R$  (dimensionless), and macroscopic activation energies  $E_M^R$  (eV) deduced from the fitting of the  $^7\text{Li}$  NMR spin-lattice ( $1/T_1$ ) relaxation data in two regions analyzed.

EC					NMR			
$T$ (K)	$E_M^C$ (eV)	$\sigma_{b,0}$ ( $\text{S cm}^{-1}$ )	$E_\omega^C$ (eV)	$\omega_{bp0}$ ( $\text{s}^{-1}$ )	$\tau_0^C$ (s) = $\omega_{bp0}^{-1}$	$\tau_0^R$ (s)	$\beta^R$	$E_M^R$ (eV)
170–250	$0.32 \pm 0.01$	$4.5 \pm 0.4 \times 10^5$	$0.31 \pm 0.01$	$8 \pm 2 \times 10^{14}$	$1.2 \pm 0.8 \times 10^{-15}$	$0.7 \pm 0.2 \times 10^{-14}$	$0.61 \pm 0.05$	$0.29 \pm 0.01$
250–450	$0.23 \pm 0.01$	$1.3 \pm 0.3 \times 10^4$	$0.23 \pm 0.01$	$1.2 \pm 0.2 \times 10^{13}$	$0.8 \pm 0.1 \times 10^{-13}$	$2 \pm 1 \times 10^{-12}$	$0.85 \pm 0.05$	$0.21 \pm 0.01$

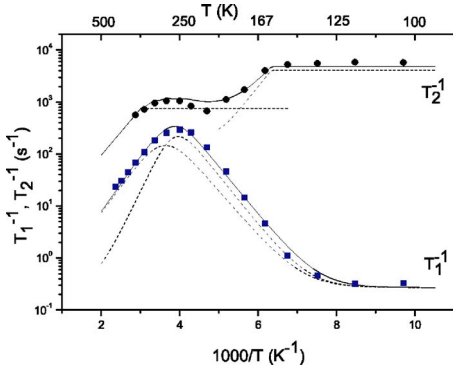


FIG. 7. (Color online) Temperature dependence of  ${}^7\text{Li}$  NMR spin-lattice ( $1/T_1$ ) and spin-spin ( $1/T_2$ ) relaxation rates of  $\text{Li}_{1.2}\text{Ti}_{1.8}\text{Al}_{0.2}(\text{PO}_4)_3$ . Experimental  $1/T_1$  data were fitted to two relaxation mechanisms described with modified BBP expressions (see text).

$$T_2^{-1} = \frac{1}{2}C' \left[ 3\tau + \frac{5\tau}{1 + (\omega_0\tau)^{1+\beta}} + \frac{2\tau}{1 + (2\omega_0\tau)^{1+\beta}} \right], \quad (4)$$

where  $C$  and  $C'$  depend on the magnetic interactions that cause the nuclear relaxation,  $\beta$  is a constant that takes into account correlation effects in the Li motion, and  $\tau$  is the residence time at the structural sites. The dependence of  $\tau$  on temperature is given by the expression

$$\tau = \tau_0^R \exp(E_M^R/kT), \quad (5)$$

where  $k$  is the Boltzmann constant,  $\tau_0^R$  is the residence time at infinite temperature, and  $E_M^R$  is the activation energy deduced from the high temperature branch of  $1/T_1$  maximum. Activation energy deduced from the low temperature side of the maximum is given by  $E_M^R\beta^R$ .

The constant  $C$ , deduced from the fitting of the  $T_1^{-1}$  plot, was  $C \approx 5 \times 10^9$  (rad/s) $^2$ .<sup>2</sup> If Li relaxation is produced by fluctuations of quadrupole interactions,  $C_Q$  (expressed in Hz) can be calculated with the expression<sup>19</sup>

$$C \approx \left( \frac{2\pi^2}{5} \right) \left( 1 + \frac{\eta^2}{3} \right) C_Q^2. \quad (6)$$

The  $C_Q$  value (38.5 KHz) deduced with expression (6) is close to the value deduced from the  ${}^7\text{Li}$  NMR spectrum recorded at 190 K (35 KHz), confirming that fluctuations of quadrupole interactions are responsible for spin-lattice relaxation. In the case of  $T_2^{-1}$  plots, the  $C'$  constant deduced from the fitting of the spectrum taken at 160 K was clearly lower,  $C' \approx 1.6 \times 10^7$  (rad/s) $^2$ , suggesting that dipolar interactions are responsible for  $T_2^{-1}$  relaxation processes.

In order to reproduce the temperature dependence of experimental  $T_1^{-1}$  and  $T_2^{-1}$  values, we have used the expressions (see Discussion section)

$$\frac{1}{T_1} = \frac{1}{T_1^{LT}} + \frac{1}{T_1^{HT}} + \frac{1}{T_1^{PAR}} \quad (7)$$

$$\frac{1}{T_2} = \frac{1}{T_2^{LT}} + \frac{1}{T_2^{HT}} + \Delta\omega, \quad (8)$$

where  $(T_1^{LT})^{-1}$ ,  $(T_2^{LT})^{-1}$  and  $(T_1^{HT})^{-1}$ ,  $(T_2^{HT})^{-1}$  stand for low and high temperature mechanisms. In the absence of lithium motion ( $T < 160$  K),  $\Delta\omega$  increase with dipolar interactions; and  $T_1^{PAR}$  decrease with paramagnetic interactions.

## IV. DISCUSSION

### A. Li sites occupancy

In order to ascertain which sites are occupied by lithium at 160 K in the Nasicon structure, the second moment  $\Delta\omega^2$  (expressed in  $\text{G}^2$ ) of the central transition of the  ${}^7\text{Li}$  NMR spectrum, recorded in static conditions, was compared with second moment values deduced for  $M_1$  and  $M_{1/2}$  sites. Second moments were calculated with the Van Vleck expression<sup>20</sup>

$$\Delta\omega^2 = \frac{3}{5} \gamma_I^4 \hbar^2 I(I+1) \sum_k \frac{1}{r_{jk}^6} + \frac{4}{15} \gamma_I^2 \gamma_S^2 \hbar^2 S(S+1) \sum_k \frac{1}{r_{jk}^6}, \quad (9)$$

where the first term accounts for dipolar interactions between like spins and the second one for interactions between unlike spins.  $\gamma_I$  and  $\gamma_S$  are the gyromagnetic ratios of  $I$  and  $S$  spins and  $r_{jk}$  is the distance between interacting spins.

In  $M_1$  sites, the contribution of Li—Li dipole interactions to  $\Delta\omega^2$  (0.11  $\text{G}^2$ ) is higher than those of Li—P (0.09  $\text{G}^2$ ) and Li—Al (0.04  $\text{G}^2$ ) interactions, but the contribution of Li—Ti interactions is negligible. The  $\Delta\omega^2$  value calculated for the  $M_1$  sites (0.24  $\text{G}^2$ ) is considerably lower than that calculated for the  $M_{1/2}$  sites (0.41  $\text{G}^2$ ), but similar to that deduced from the central line of the  ${}^7\text{Li}$  NMR spectrum (0.22  $\text{G}^2$ ). Similar conclusions are obtained from the analysis of satellite transitions. In  $M_1$  sites the  $C_Q$  constant (15 KHz) is considerably lower than that deduced for the midway  $M_{1/2}$  sites ( $\sim 120$  KHz), but near that deduced from NMR satellite transitions (35 KHz).<sup>21,22</sup> According to this analysis, most of the Li occupy sites with axial symmetry ( $M_1$  sites) at 160 K. These sites located at the intersection of three conduction channels strongly condition Li motion in the structure of these compounds.

When  $\text{Li}_{1.2}\text{Ti}_{1.8}\text{Al}_{0.2}(\text{PO}_4)_3$  is heated above 160 K (Fig. 7),  $T_2^{-1}$  decreases as a consequence of lithium mobility. In order to explain the spectral narrowing, the residence time at occupied  $M_1$  sites should be lower than the linewidth inverse recorded at 160 K; it is  $3 \times 10^{-4}$  s ( $\tau \leq 1/\Delta\omega$ ). The decrease of  $T_2^{-1}$  is accompanied by an increase of  $C_Q$  (Fig. 6). This trend, which is opposite to that expected for lithium hopping between equivalent sites, indicates that other sites different from  $M_1$ , probably  $M_{1/2}$  sites, are involved in Li hopping. The occupancy of  $M_{1/2}$  sites increase Li—P interactions and explains the increase of  $T_2^{-1}$  values detected between 210 and 250 K. When residence time at  $M_1$  and  $M_{1/2}$  sites decreases, dipolar interactions decrease again, producing the spectral narrowing detected at high temperatures ( $T > 300$  K).

If we assume that lithium exchanges between  $M_1$  and midway  $M_{1/2}$  sites, the observed  $C_Q$  values can be calculated with the expression<sup>21</sup>

$$C_Q = \frac{C_Q^1 P_1 + C_Q^2 3P_2}{P_1 + 3P_2}, \quad (10)$$

where  $C_Q^1$  and  $C_Q^2$  are the quadrupole constants, and  $P_1$  and  $P_2$  are the occupation probabilities of  $M_1$  and  $M_{1/2}$  sites. The factor 3 takes into account the multiplicity of the  $M_{1/2}$  sites with respect to the  $M_1$  sites. The existence of fast exchange processes between both sites makes that only one signal with axial symmetry ( $\eta=0$ ) is detected.

The monotonic increase of  $C_Q$  with temperature indicates that the residence time at  $M_{1/2}$  (probability  $P_2$ ) increases at expenses of the residence time at  $M_1$  sites (probability  $P_1$ ). Experimental  $C_Q$  values can be reproduced by assuming that  $C_Q$  constants of  $M_1$  and  $M_{1/2}$  sites are 15 and 120 kHz, respectively,<sup>21,22</sup> (see Table I). From the analysis of these values, it can be concluded that below 200 K most  $M_1$  sites are occupied, but only a part of  $M_{1/2}$  sites are occupied by Li ions ( $C_Q=35$  kHz). At higher temperatures, Li ions are transferred from  $M_1$  to  $M_{1/2}$  sites, increasing the amount of vacancies at  $M_1$  sites (see Table I). The analysis of the temperature dependence of sites occupancy indicates that creation of vacancies at  $M_1$  sites is an activated process with an activation energy near 0.07 eV. This value agrees with the difference of activation energies outlined in Table II for the low and high temperature regimes (Fig. 5). In samples heated at 450 K, 2/3 of  $M_1$  sites are occupied by lithium, indicating that the full vacancy disordering,  $P_1=P_2=0.3$  ( $C_Q \approx 100$  kHz), is not attained in the temperature range 200–500 K.

### B. Li mobility

In general, Li mobility produces a decrease of the line-width of NMR spectra ( $1/T_2$ ) and a maximum in  $T_1^{-1}$  as temperature increases. In the case that ions occupy two structural sites, two different  $1/T_1$  and  $1/T_2$  values could be detected. However, in the fast ion conductor studied,  $\text{Li}_{1.2}\text{Ti}_{1.8}\text{Al}_{0.2}(\text{PO}_4)_3$ , exchange processes between structural sites average these values, producing the detection of only one type of lithium with intermediate characteristics. In this case,  $1/T_1$  and  $1/T_2$  values are given by equations

$$1/T_1 = n_1 1/T_1^{(1)} + n_{1/2} 1/T_1^{(1/2)}, \quad (11)$$

$$1/T_2 = n_1 1/T_2^{(1)} + n_{1/2} 1/T_2^{(1/2)}, \quad (12)$$

where  $n_1=P_1$  and  $n_{1/2}=3P_2$  stand for the relative amount of Li at  $M_1$  and  $M_{1/2}$  sites. In these expressions  $n_1$  and  $n_{1/2}$  change as a function of temperature (see Table I).

A deeper analysis of  $T_2^{-1}$  vs  $1000/T$  shows a decrease in two-stages: one between 160 and 210 K and other above 300 K. Moreover, the  $T_1^{-1}$  maximum is broader than that expected for a single BPP mechanism. Therefore the fitting of  $T_2^{-1}$  and  $T_1^{-1}$  values requires more than one relaxation mechanism (Fig. 7). In accordance with these results, the dependences of the grain interior conductivity  $\sigma_{b,dc}$  and the fre-

quency  $\omega_{bp}$  vs inverse temperature (Fig. 5) show deviations from the Arrhenius behavior that can be described with two linear dependences. The activation energy  $E_M^C$  decreases from 0.31 eV for the low temperature regime to 0.23 eV for the high temperature regime. A departure from the Arrhenius behavior has also been observed in glassy ionic conductors showing dc conductivities close to  $10^{-2}$  S  $\text{cm}^{-1}$ . However, this departure has not been observed in poor ionic conductors, in which high conductivity values cannot be reached at temperatures below the glass transition.<sup>3</sup>

For the low temperature branch of  $T_1^{-1}$ , the activation energy deduced from NMR data is  $E_m^R \approx 0.19$  eV. However, the activation energy deduced from conductivity data in the same temperature range is  $E_M^C=0.31$  eV, suggesting the presence of correlation effects in the lithium motion. If it is assumed that  $E_M^C=E_M^R$  in the low temperatures regime, it is possible to deduce the correlation factor<sup>1,23</sup>  $\beta^R=E_m^R/E_M^R \approx 0.61$ . This factor is appreciably higher than that deduced from the modulus peak at 223 K,  $\beta^C \approx 0.5$ . For the high temperature branch of  $T_1^{-1}$ , the activation energy deduced ( $E_m^R=0.21$  eV) is almost coincident with that deduced from conductivity data in the same temperature range ( $E_M^C=0.23$  eV). This value is also similar to the activation energy deduced from the low temperature side of  $T_1^{-1}$  maximum ( $E_m^R=0.19$  eV); indicating that correlation effects have decreased and factor  $\beta^R$  deduced above 375 K is  $\sim 0.9$ . Unfortunately,  $\beta^C$  values deduced from the modulus peaks cannot be obtained for  $T>320$  K; however, an extrapolation of  $\beta^C$  values at 400 K gives  $\beta^C=0.8$ , that are similar to that deduced from NMR fitting of  $T_1^{-1}$  data ( $\beta^R \approx 0.85$ ). Therefore the Li motion changes from a correlated motion in the low temperature regime to a much less correlated motion in the high temperature regime. This conclusion is supported by the narrowing of the  $M''$  peaks detected at increasing temperatures (see Fig. 4 and Table I).

Taking into account the expression  $E_M^C=E_m^C/\beta^C$ , the increment of  $\beta^C$  would be responsible for the decrease observed in  $E_M^C$  values in Fig. 5. Taking into account that the  $\beta^C$  parameter should not change in each mechanism, the continuous variation of  $\beta^C$  must be apparent and results from the average of two relaxation processes whose relative importance changes in the temperatures range 200–400 K.

An explanation for changes detected on the  $\beta^C$  parameter could be the increment of vacant  $M_1$  sites as temperature increases. As stated previously, the creation of vacancies at  $M_1$  sites is activated with an activation energy near 0.07 eV. This value agrees with the difference between low- and high-temperature activation energies outlined in Table II for the two Li-motion regimes. The creation of vacancies at the intersection of conduction channels ( $M_1$  sites) opens new conduction pathways that will favor an important decrease on correlation effects, i.e., an increase on  $\beta^C$ , and an important decrease on activation energy  $E_M^C$ . A similar effect was invoked in the  $\text{Li}_{1+x}\text{Ti}_{2-x}\text{Al}_x^{3+}(\text{PO}_4)_3$  series, where an increment of the Li content improved electrostatic Li—Li interactions, increasing the amount of vacant  $M_1$  sites. In this case activation energy  $E_M^C$ , measured at room temperature, decreased from 0.45 to 0.3 eV when  $x$  increased from 0 to 0.2.

At this point, it is interesting to analyze the temperature dependence of the correlation times of low- and high-

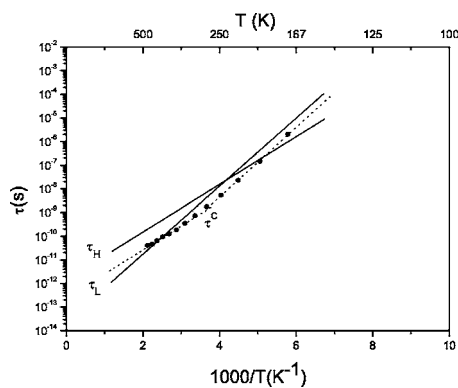


FIG. 8. Temperature dependence of the relaxation time  $\tau^C = \omega_{bp}^{-1}$  deduced from electric modulus  $M''$  peaks (closed circles), and NMR correlation times  $\tau_L^R$  and  $\tau_H^R$  deduced from spin-lattice ( $1/T_1$ ) relaxation data. The dashed line is given to guide the eye.

temperature mechanisms ( $\tau_L^R$  and  $\tau_H^R$ ) deduced from the fitting of the  $T_1^{-1}$  curve. Two straight lines with different slopes are detected (Fig. 8). In this figure, residence times  $\tau^C$  deduced from electric modulus peak have been included (closed circles). The temperature dependences of  $\tau_L^R$ ,  $\tau_H^R$ , and  $\tau^C$  are similar, however, correlation times deduced from electric data are systematically lower than those deduced from NMR measurements. Similar results have been reported by Blache *et al.*<sup>23</sup> in lithium silicophosphate glasses, indicating that the spectral density function, describing relaxation processes, can be slightly different in the two techniques.

Finally, it is interesting to analyze the temperature dependence of the correlation times. It is seen that  $\tau_L^R$  and  $\tau_H^R$  lines cross near 250 K indicating that two relaxation mechanisms coexist in the range 200–350 K and that a change of regime is produced. Extrapolated values at infinite temperatures are  $\tau_{L,0}^R = 7 \times 10^{-15}$  s for the first mechanism and  $\tau_{H,0}^R = 2 \times 10^{-12}$  s for the second one. Similar conclusions can be derived from conductivity data. However,  $\tau_{L,0}^C$  and  $\tau_{H,0}^C$  values extrapolated from electrical measurements are about 1 order of magnitude lower than those deduced from NMR results.

An estimation of diffusion coefficients  $D$  can be done through the equation

$$D = \frac{a_0^2}{6\tau^R} \quad (13)$$

where  $a_0 \sim 3.5$  Å is the mean distance between  $M_1$  and  $M_{1/2}$  sites related by hopping and  $\tau^R$  is the correlation time for a

given temperature. At the maximum of the  $T_1^{-1}$  plot,  $\tau^R \approx 1.4 \times 10^{-8}$  s, we obtain  $D \approx 1.5 \times 10^{-12}$  m<sup>2</sup> s<sup>-1</sup> that is one of the highest values reported at 250 K in crystalline Li-ion conductors. According to this fact, it is also possible to deduce diffusion coefficients as a function of temperature. For that,  $\tau_H^R$  values deduced from NMR data should be used with Eq. (13), resulting in the expression

$$D = \frac{a_0^2}{6\tau_{H,0}^R R} e^{-E_M^R/kT} = 1 \times 10^{-8} e^{-0.19/kT} \text{ m}^2 \text{ s}^{-1}.$$

## V. CONCLUSIONS

Local structure and lithium mobility in  $\text{Li}_{1.2}\text{Ti}_{1.8}\text{Al}_{0.2}(\text{PO}_4)_3$  has been analyzed with XRD, NMR, and electric impedance techniques. From the frequency dependence of conductivity, the grain interior (bulk) and grain boundary contributions were determined as a function of temperature.

The preferential occupancy of  $M_1$  sites was deduced from the analysis of dipolar and quadruple interactions in the  $^7\text{Li}$  NMR spectra recorded at 160 K. The variation of  $T_2^{-1}$  and  $C_Q$  values with temperature showed the progressive occupancy of midway  $M_{1/2}$  sites at expenses of  $M_1$  sites as the temperature increases. From the temperature dependence of  $T_1^{-1}$  and  $T_2^{-1}$ , two different regimes associated with correlated and noncorrelated motions have been deduced. In both regimes, the activation energy  $E_m^R$  is 0.19 eV.

Activation energy of lithium motion decreases when temperature increases, producing an appreciable deviation from the Arrhenius behavior in dc-conductivity data. The decrease observed in  $E_M^C$  from 0.31 to 0.21 eV has been ascribed to the partial cancellation of correlation effects produced by the creation of vacancies at  $M_1$  sites. According to this fact, activation energies  $E_M^C$  and  $E_M^R$ , deduced from conductivity and NMR measurements in the temperature range 300–450 K, almost coincides with the activation energy  $E_m^R$  deduced from NMR at low temperatures (0.19 eV).

## ACKNOWLEDGMENTS

Financial support provided by Spanish CICYT, Projects MAT2001-0562 and MAT2004-3070-CO5 is acknowledged. K. Arbi and M. G. Lazarraga thank Spanish Ministry of Science and Technology, and Ministry of Education, Culture and Sport for the financial support.

\*Corresponding author. Email address: jsanz@icmm.csic.es

<sup>1</sup>K. L. Ngai, Phys. Rev. B **48**, 13481 (1993).

<sup>2</sup>K. L. Ngai and A. K. Rzos, Phys. Rev. Lett. **76**, 1296 (1996).

<sup>3</sup>A. D. Robertson, A. R. West, and A. G. Ritchie, Solid State Ionics **104**, 1 (1997).

<sup>4</sup>H. Aono, E. Sugimoto, Y. Sadaoka, N. Imanaka, and G.-Y. Adachi, J. Electrochem. Soc. **137**, 1023 (1990).

<sup>5</sup>S. Wong, P. J. Newman, A. S. Best, K. M. Nairn, D. R. MacFar-

lane, and M. Forsyth, J. Mater. Chem. **8**, 2199 (1998).

<sup>6</sup>K. Arbi, S. Mandal, J. M. Rojo, and J. Sanz, Chem. Mater. **14**, 1091 (2002).

<sup>7</sup>E. Morin, J. Angenault, J. C. Couturier, M. Quarton, H. He, and J. Klinowski, Eur. J. Solid State Inorg. Chem. **34**, 947 (1997).

<sup>8</sup>E. R. Losilla, M. A. G. Aranda, M. Martinez-Lara, and S. Bruque, Chem. Mater. **9**, 1678 (1997).

<sup>9</sup>M. Catti, S. Stramare, and R. Ibberson, Solid State Ionics

- 123**, 173 (1999).
- <sup>10</sup>A. Aatiq, M. Ménétrier, L. Croguenne, E. Suard, and C. Delmas, *J. Mater. Chem.* **12**, 2971 (2002).
- <sup>11</sup>K. Arbi, M. G. Lazarraga, D. B. Chehimi, M. Ayadi-Trabelsi, J. M. Rojo, and J. Sanz, *Chem. Mater.* **16**, 255 (2004).
- <sup>12</sup>D. Massiot, WINFIT, Bruker-Franzen Analytik GmbH, Bremen, Germany, 1993.
- <sup>13</sup>J. Ross Macdonald, in *Impedance Spectroscopy. Emphasizing Solid Materials and Systems* (Wiley, New York, 1987).
- <sup>14</sup>C. T. Moynihan, L. P. Boech, and N. L. Laberge, *Phys. Chem. Glasses* **14**, 122 (1973).
- <sup>15</sup>F. Borsa, D. R. Torgeson, S. W. Martin, and H. K. Patel, *Phys. Rev. B* **46**, 795 (1992).
- <sup>16</sup>H. Jain, *J. Non-Cryst. Solids* **66**, 517 (1984).
- <sup>17</sup>M. Grüne and W. Müller-Warmuth, *Ber. Bunsenges. Phys. Chem.* **95**, 1068 (1991).
- <sup>18</sup>O. Kanert, R. Küchler, K. L. Ngai, and H. Jain, *Phys. Rev. B* **49**, 76 (1994).
- <sup>19</sup>A. Abragam, *The Principles of Nuclear Magnetic* (Oxford University Press, Oxford, 1961).
- <sup>20</sup>J. H. Van Vleck, *Phys. Rev.* **74**, 1168 (1948).
- <sup>21</sup>M. A. París, A. Martínez-Juárez, J. M. Rojo, and J. Sanz, *J. Phys.: Condens. Matter* **8**, 5355 (1996).
- <sup>22</sup>M. A. París and J. Sanz, *Phys. Rev. B* **62**, 810 (2000).
- <sup>23</sup>V. Blache, J. Förster, H. Jain, O. Kanert, R. Küchler, and K. L. Ngai, *Solid State Ionics* **113–115**, 723 (1998).